




Observation of orthopositronium thermalization in silica aerogel at cryogenic temperaturesKenji Shu ,* Akira Ishida ,† Toshio Namba, and Shoji Asai *Department of Physics, Graduate School of Science, and International Center for Elementary Particle Physics, The University of Tokyo, 7-3-1 Hongo, Bunkyo-ku, Tokyo 113-0033, Japan*Nagayasu Oshima , Brian E. O'Rourke , and Kenji Ito *National Institute of Advanced Industrial Science and Technology (AIST), Tsukuba-Central 2, 1-1-1 Umezono, Tsukuba, Ibaraki 305-8568, Japan*

(Received 21 July 2021; revised 22 October 2021; accepted 11 November 2021; published 24 November 2021)

We report *ortho*positronium (*o*-Ps) thermalization observed in cryogenic silica aerogel cooled from room temperature to 25 K. It was observed that the *o*-Ps thermalization rate gets slower as *o*-Ps itself is colder than room temperature. This energy dependence can be explained based on a model where the efficiency of kinetic energy exchange between *o*-Ps and silica is determined by the de Broglie wavelength of *o*-Ps. The present measurement confirmed that a cooling method which utilizes the thermalization process at cryogenic temperatures followed by laser cooling is applicable for the efficient production of an *o*-Ps Bose-Einstein condensate.

DOI: [10.1103/PhysRevA.104.L050801](https://doi.org/10.1103/PhysRevA.104.L050801)

Positronium (Ps), the bound state of an electron and a positron, is a good probe for fundamental physics. Due to its simple and purely leptonic structure, Ps has been applied for high precision tests on bound-state quantum electrodynamics [1–5] and also used in highly sensitive searches on physics beyond the standard model of particle physics [6]. One of the most interesting Ps experiments performed recently is the fine structure ($2S$ – $2P$ energy interval) measurement [7,8] which revealed unresolved 4.2σ discrepancy between experimental and theoretical values. Another significant feature of Ps is that it contains antimatter and may be considered the simplest system containing both antimatter and matter. Searches for matter-antimatter asymmetry have been performed with Ps [9], including in the gravity sector [10–13], where experiments to measure the effect of gravity on anti-hydrogen are in progress [14–17]. One of the desired future breakthroughs on Ps study is the production of sufficient quantities of cold *ortho*-Ps (*o*-Ps), a spin-triplet state with a relatively long lifetime in vacuum (142 ns) [4]. Cryogenic *o*-Ps at less than 10 K can enable a measurement of the *o*-Ps $1S$ – $2S$ energy interval to an order of magnitude precision higher than existing measurements [2] due to the narrower Doppler broadening. The precision of $2S$ – $2P$ measurement may also be improved by cold *o*-Ps and subsequent $1S$ – $2S$ two-photon transition which can be used for efficient production of Ps in the $2S$ state. More interestingly, a Bose-Einstein condensate (BEC) of a system containing antimatter can be realized with high density, cryogenic *o*-Ps cooled down to 10 K [11,18–23].

Recently, we proposed a Ps cooling method, a combination of thermalization and subsequent laser cooling by $1S$ – $2P$ transitions, for realizing Ps-BEC [19]. In this method, *o*-Ps is confined in a cold, porous SiO_2 (silica) cavity. In the thermalization cooling, the kinetic energy of *o*-Ps is transferred to the silica matrix via interactions with the cavity walls, so *o*-Ps thermalizes to a temperature comparable to silica. Unfortunately, the evaluation of the Ps cooling efficiency of the thermalization has large uncertainty [19,20] because the time evolution of the kinetic energy of Ps confined in a silica cavity has never been observed below room temperature. It is necessary for the estimation to extrapolate the effective mass of silica M , which is the mass of silica bodies scattering with *o*-Ps in the classical elastic collision model [24] and is the most important parameter for the calculation of the Ps cooling efficiency to cryogenic temperatures. Although the best-fit extrapolation used in our cooling simulation showed sufficient efficiency for realizing Ps-BEC, the most pessimistic scenario showed that our cooling method could not cool Ps down to the BEC critical temperature [20]. For the proposed cooling method, it is important to determine how fast Ps loses its kinetic energy below room temperature.

Several previous experiments [24–27] have measured M , but all were performed at temperatures higher than room temperature. Other experiments [28–30] created Ps in cryogenic silica materials, but only part of the created Ps had a cryogenic temperature and the rest did not. A quantum confinement effect is one of the reasons for the limited thermalization to the cryogenic temperatures. This effect arises when the thermal de Broglie wavelength of Ps $\lambda_{\text{Ps}}^{\text{dB}}$ is as large as the size of cavities confining Ps. Because the mass of Ps m_{Ps} is quite small, $\lambda_{\text{Ps}}^{\text{dB}}$ is quite large, i.e., $\lambda_{\text{Ps}}^{\text{dB}} = 0.60 \text{ nm} \sqrt{1 \text{ eV}/E} = 53 \text{ nm} \sqrt{1 \text{ K}/T_{\text{Ps}}}$, where E is the average kinetic energy of Ps and T_{Ps} is the Ps temperature calculated with the Boltzmann constant k_B as $T_{\text{Ps}} = 2E/3k_B$. The minimum kinetic energy of confined Ps is limited such that $\lambda_{\text{Ps}}^{\text{dB}}$ is smaller than the cavity size [31–33].

*Present address: Photon Science Center, Graduate School of Engineering, The University of Tokyo, 2-11-16 Yayoi, Bunkyo-ku, Tokyo 113-8656, Japan.

†Corresponding author: ishida@icepp.s.u-tokyo.ac.jp

Another aspect of the quantum confinement effect is expected to slow down or eventually stop the thermalization process if intervals of quantized kinetic energy in nanocavities exceed the maximum kinetic energy loss via a collision with the cavity walls [31]. Although larger cavities are better for *o*-Ps thermalization to avoid the quantum confinement effect, the rate of collisions between *o*-Ps and the cavity walls are decreased; as a result, complete thermalization requires longer time. These conflicting effects make it difficult to accurately estimate the efficiency of the Ps thermalization cooling at cryogenic temperatures solely based on the data obtained at higher temperatures.

In this Letter, the thermalization process of *o*-Ps confined in cryogenic porous silica was observed and M involved with *o*-Ps at cryogenic temperatures was analyzed based on a model introducing a quantum size effect of *o*-Ps. A method used in other Ps thermalization measurements [34,35], what we call pick-off technique hereafter, is chosen to measure the Ps thermalization and M because this technique has the advantage that it does not require any additional elements such as gases or magnetic field which shorten the *o*-Ps lifetime.

Pick-off annihilation occurs when the positron forming an *o*-Ps particle overlaps with an electron belonging to the surrounding materials (silica in this Letter). The pick-off annihilation rate Γ_2 depends both on the mean-free path L of the collisions and the size of Ps [36–38]. The dependence of Γ_2 on the Ps temperature T_{Ps} can be estimated according to the rectangular Tao-Eldrup (RTE) model [37]. The model assumes that *o*-Ps is confined in a three-dimensional rectangular cavity, in which *o*-Ps within a distance $\delta \approx 0.18$ nm from the material wall annihilates with a spin-averaged annihilation rate $\approx 8 \times 10^3 \mu\text{s}^{-1}$ [4,5]. Although silica cavities used in the present Letter should have more complex shapes than rectangular with a wide variation, the RTE model is used here since any effects on the pick-off annihilation rate from specific morphology of the cavity have not been pointed out so far. The time evolution of Γ_2 is measured and converted into T_{Ps} by the RTE model in this Letter.

Figure 1 shows a schematic diagram of the experimental setup. A 250 kBq ^{22}Na radioisotope was used as a positron source. A silica aerogel block (0.11 g cm $^{-3}$, $32 \times 32 \times 10$ mm 3) attached to the cold head of a 4 K GM refrigerator was used as a converter to trap Ps in its pores. The mean-free path of Ps confined in the aerogel was calculated as $L = 38.47(71)$ nm from the specific surface area S/V , where S is the total surface area and V is the bulk volume, of the aerogel measured by the Brunauer-Emmett-Teller (BET) method [39] as $S/V = 9.88 \times 10^7$ m $^{-1}$. Here we used the relationship $L = 4V/S$, which is known to hold for three-dimensional void structures without assuming a specific morphology in the aerogel. The obtained L reasonably agrees with the pore size for the aerogel, which distributed from 20 nm to 50 nm based on electron microscope images, although we did not use the pore size in the calculation because estimating L from the pore size requires the real dimension of the pores which may involve a large uncertainty to the estimation. The output power of the heater on the refrigerator was controlled so the temperature of the aerogel T_{env} was adjustable from 25 K to 295 K, which was monitored by silicon sensors and fed back to the controlling system. The base pressure of the vacuum chamber was 2×10^{-5} Pa, which went down to 2×10^{-6} Pa while the refrigerator was running. Measurements were per-

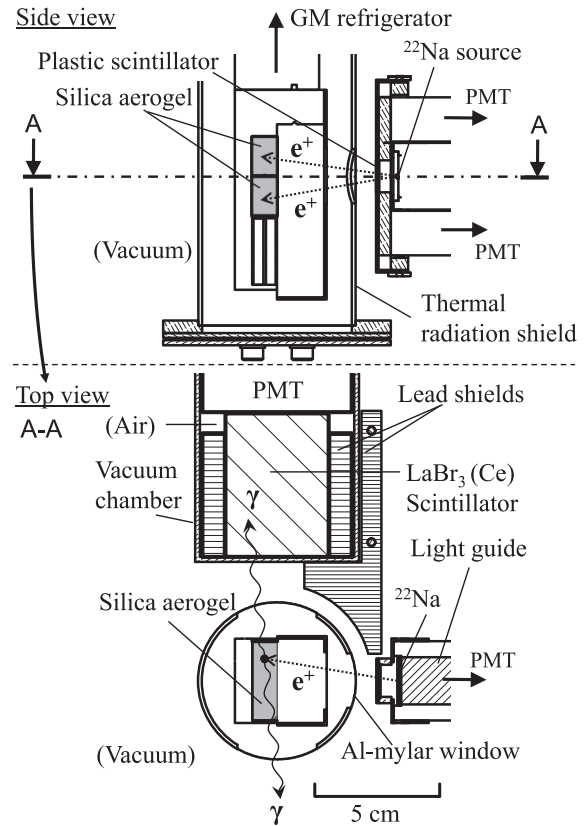


FIG. 1. Schematic view of the experimental setup inside the vacuum chamber. PMTs and the $\text{LaBr}_3(\text{Ce})$ scintillator are located outside the vacuum chamber.

formed at four T_{env} of 295 K, 210 K, 130 K, and 25 K. The data at the former three T_{env} were recorded for two weeks, while the data at 25 K were recorded for one month through measuring three times after the same thermal cycle: heating the silica aerogel to room temperature and cooling it down to 25 K. The data acquisition was carried out very stably, and any fluctuations due to the gas adsorption to the aerogel block were not observed.

A 200- μm -thick plastic scintillator was placed between the positron source and the silica aerogel to tag the timing of positron emission, which was almost simultaneous with the subsequent formation of Ps. Annihilation γ rays were detected by a $\text{LaBr}_3(\text{Ce})$ scintillator ($\varnothing 38.1$ mm \times 50.8 mm) whose head was 6 cm away from the center of the aerogel target. Data acquisition was triggered by coincident signals in both the positron and γ -ray detectors, enabling us to record the energy and timing information of each event. The time resolution was 2.2 ns full width at half-maximum (FWHM) and the energy resolution at 511 keV was 4.6% FWHM. Signal processing and recording were performed by NIM and CAMAC systems. The whole experimental system was coded in a GEANT4 Monte Carlo (MC) simulator [40–42] to evaluate detection efficiencies for positrons and γ rays.

Data analysis similar to that described previously [22,34,35] was conducted to deduce the time evolution of Γ_2 . Histograms of the time intervals t between positron emission and detection of the annihilation γ ray were processed to evaluate timing spectra. A pileup rejection was

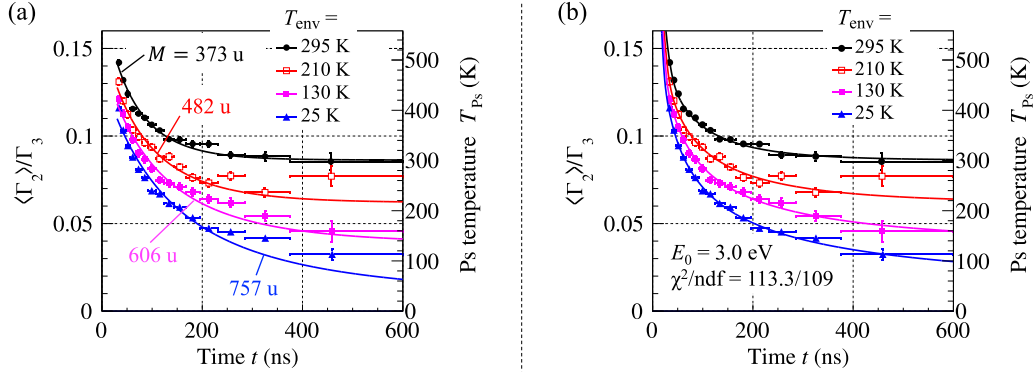


FIG. 2. Time evolution of $\langle \Gamma_2 \rangle$ with the various T_{env} . $\langle \Gamma_2 \rangle$ is normalized to Γ_3 on the left vertical axis. The right vertical axis shows T_{Ps} , which is converted from $\langle \Gamma_2 \rangle$ by the RTE model. The markers are obtained by Eq. (1) whose N are calculated by the experimental energy spectra. Horizontal bars show timing ranges to produce the spectra for corresponding markers. Vertical error bars show statistical uncertainties. Fitting curves are superimposed by solid lines calculated by Eq. (2) and the RTE model. The separate measurements at 295 K (twice) and 25 K (three times) are treated independently in the calculation of $\chi^2/n\text{dof}$, whereas the markers show averaged values at the same T_{env} . (a) $M(E) = \text{const}$ for each T_{env} (u: unified atomic mass unit). (b) Fitting Eq. (5) to all the data globally.

applied in processing t to prevent distortion of the timing spectra described in Ref. [43]. *o*-Ps annihilation events were selected from $t = 30$ –600 ns, and accidental events estimated from $t = 1250$ –1500 ns were subtracted. The validity of the subtracted energy spectra was checked by comparing them with the respective MC spectra with an appropriate scale and a detector response function which included calibration factors and the energy resolution.

To calculate Γ_2 , two energy regions are defined. One from 350–470 keV is dominated by *o*-Ps 3γ self-annihilation events which have a continuous energy spectrum up to 511 keV. The other from 480–540 keV effectively collects 2γ pick-off annihilation events with 511 keV monoenergetic γ rays. Counts within a timing window (t_1, t_2) in the 3γ region $N_3(t_1, t_2)$ and in the 2γ region $N_2(t_1, t_2)$ are then sensitive to rates of self-annihilation and pick-off annihilation, respectively, between $t = t_1$ and $t = t_2$. The average pick-off annihilation rate $\langle \Gamma_2 \rangle$ in the timing windows are calculated by the following equation:

$$\begin{cases} N_3(t_1, t_2) = \int_{t_1}^{t_2} dt' [\varepsilon_{33}\Gamma_3 + \varepsilon_{23}\Gamma_2(t')]N(t') \\ N_2(t_1, t_2) = \int_{t_1}^{t_2} dt' [\varepsilon_{22}\Gamma_2(t') + \varepsilon_{32}\Gamma_3]N(t') \end{cases}$$

$$\begin{aligned} \rightarrow \frac{\langle \Gamma_2 \rangle(t_1, t_2)}{\Gamma_3} &= \frac{\int_{t_1}^{t_2} dt' \Gamma_2(t')N(t')}{\int_{t_1}^{t_2} dt' \Gamma_3 N(t')} \\ &= \frac{\varepsilon_{33}N_2(t_1, t_2) - \varepsilon_{32}N_3(t_1, t_2)}{\varepsilon_{22}N_3(t_1, t_2) - \varepsilon_{23}N_2(t_1, t_2)}, \quad (1) \end{aligned}$$

where $N(t)$ is the remaining number of *o*-Ps at time t , $\Gamma_3 = 7.0401(7) \mu\text{s}^{-1}$ [4] is the *o*-Ps self-annihilation rate in vacuum which does not depend on T_{Ps} or t , and ε_{mn} are detection efficiencies for $m\gamma$ annihilation events in the $n\gamma$ region. The efficiencies are calculated by the 2γ and 3γ spectra generated by the MC simulation. The uncertainty of ε_{mn} is evaluated as 3% by a radioisotope whose γ -ray spectrum is known.

Figure 2 shows the time evolution of $\langle \Gamma_2 \rangle$ and T_{Ps} at each of the measured T_{env} . The data clearly show that $\langle \Gamma_2 \rangle$ gradually

decreases, and it is smaller as T_{env} is reduced. Cooling of Ps down to around 100 K is achieved in 600 ns at $T_{env} = 25$ K. The classical elastic collision model was used to fit the measured time evolution of $\langle \Gamma_2 \rangle$ to determine M . The time evolution of the average kinetic energy of *o*-Ps $E(t)$ is calculated by the following differential equation [24]:

$$\frac{dE(t)}{dt} = -\frac{2}{LM} \sqrt{2m_{Ps}E(t)} \left[E(t) - \frac{3}{2}k_B T_{env} \right]. \quad (2)$$

Equation (2) represents the following essential properties of Ps thermalization: the energy loss rate is proportional to the Ps collision rate with the cavity walls as $-dE(t)/dt \propto \sqrt{2m_{Ps}E(t)}/L = v(t)/L$, where $v(t)$ is the Ps velocity, and the Ps kinetic energy approaches the average thermal energy of $3k_B T_{env}/2$. The pick-off annihilation rate $\Gamma_2(t)$ by the RTE model is calculated as $\Gamma_2(t) = \Gamma_2^{\text{RTE}}(L, \delta, T_{Ps}(t))$. The data in Fig. 2 show the measured pick-off annihilation rate $\langle \Gamma_2 \rangle_{\text{meas}}$ of unthermalized *o*-Ps is always higher than the pick-off annihilation rate of completely thermalized *o*-Ps $\Gamma_{2,\text{therm}}^{\text{RTE}}$ calculated at $T_{Ps} = T_{env}$ by the RTE model, and $\langle \Gamma_2 \rangle_{\text{meas}}$ gradually approaches to $\Gamma_{2,\text{therm}}^{\text{RTE}}$. The data at $T_{env} = 295$ K also clearly show the agreement between $\langle \Gamma_2 \rangle_{\text{meas}}$ of completely thermalized *o*-Ps and $\Gamma_{2,\text{therm}}^{\text{RTE}}$. From these results, we can justify the adoption of the RTE model in our analysis, and our sample can be said to be free from possible effects, e.g., contaminants as reported in some porous silica samples [44], which alter the estimation based on the RTE model. $E(t)$ is treated as a continuous value since the quantization of the kinetic energy for confined Ps is typically around 6×10^{-5} eV with the pore size and the RTE model. The estimated temperature increase of the aerogel caused by *o*-Ps thermalization calculated with thermal properties of the silica aerogel [45] is less than 1 K after 10 ns from Ps formation, which makes it reasonable to treat T_{env} as a constant in Eq. (2). In Fig. 2(a), M is set to a constant value for each T_{env} to easily see the tendency of the Ps kinetic energy dependence on M , and δ is fixed to 0.1866 which is obtained by the global-fitting method described later. The chi-square method is used for the fitting. Best-fit curves are superimposed in Fig. 2(a), and obtained M are shown in

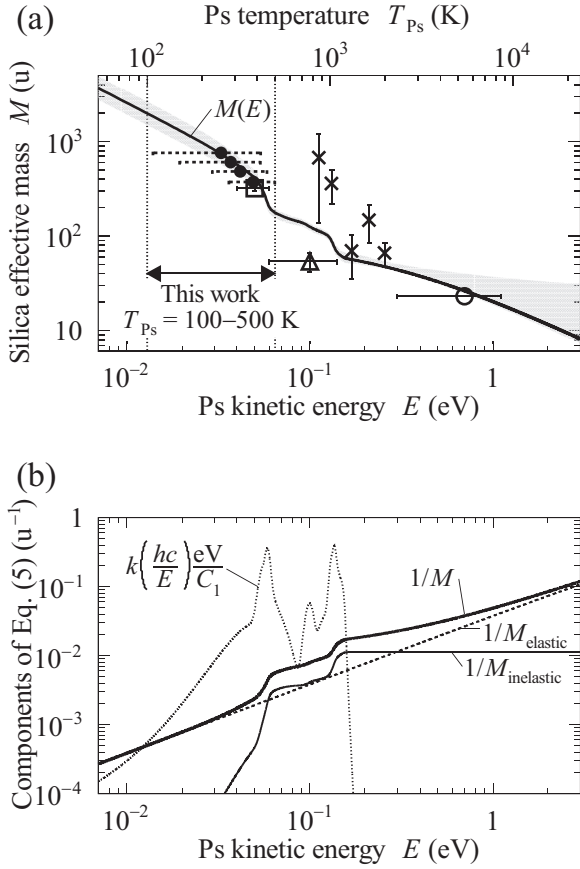


FIG. 3. (a) M for the kinetic energy exchanges with o -Ps. Markers \bullet with dashed error bars show the fitting result by the constant M for each T_{env} . Horizontal positions of the markers and the error bars are determined by the weighted mean and the range, respectively, of E or T_{Ps} for corresponding measurements. The markers with solid error bars are from the previous experiments which are included in the global fitting; \triangle , Ref. [25]; \circ , Ref. [24]; \times , Ref. [26]; \square , Ref. [27]. Both horizontal and vertical uncertainties were used to calculate chi-square. L are estimated by the o -Ps annihilation lifetime and the RTE model for experiments which did not report L explicitly. The solid line shows a center value of the fitting by Eq. (5) and an adjoining gray band shows a 1σ combined uncertainty range with statistical and systematic uncertainties. (b) Each component of Eq. (5). The integrand of $1/M_{\text{inelastic}}$ is also superimposed.

Fig. 3(a) by solid circle markers. It is found that M increases for colder Ps.

To quantitatively explain the observed cooling process, we introduce a simple phenomenological model which includes the energy dependence of the o -Ps thermalization efficiency. This model considers an inelastic scattering process and a quantum size effect on elastic scatterings by assigning the energy dependence of M in Eq. (2), in which we simply added a term $1/M_{\text{inelastic}}(E)$ to $1/M$, a factor to determine the efficiency of o -Ps thermalization with T_{env} . Although this is the lowest order approximation, it represents essential properties of Ps thermalization explained just after Eq. (2), and allows us to quantitatively reproduce the observed cooling process from around room temperature down to the cryogenic temperatures as discussed later. It is assumed here that o -Ps

can excite all the single-photon absorption modes of silica so the contribution of the inelastic scattering is assumed to be proportional to the photon absorption cross section as

$$M_{\text{inelastic}}(E) = C_1 \left[\int_0^E k \left(\frac{hc}{E'} \right) dE' \right]^{-1}, \quad (3)$$

where C_1 is a constant, h is the Planck's constant, and $k(\lambda)$ is the photon absorption index of silica glass at the wavelength λ [46]. On the other hand, the contribution of the elastic scattering is assumed to be

$$M_{\text{elastic}}(E) = M_0 + \frac{C_2}{E}, \quad (4)$$

where M_0 and C_2 are constants. The $1/E$ term can be attributed to the quantum size effect of Ps. o -Ps interacts with several atoms which make up the cavity wall of the silica aerogel naively within the size of $\approx (\lambda_{\text{Ps}}^{\text{dB}})^2 \propto 1/E$. This quantum size effect may be observable especially for Ps because of the large $\lambda_{\text{Ps}}^{\text{dB}}$ which is the same for the quantum confinement effect, but the underlying physical mechanisms of these two effects are different. In our aerogel, the quantum confinement effect would not be significant because the o -Ps mean-free path L is 3.6 times longer than $\lambda_{\text{Ps}}^{\text{dB}} = 11$ nm even at $T_{\text{Ps}} = 25$ K. From Eqs. (3) and (4), $M(E)$ is modeled as the following equation for fitting globally to the data:

$$\frac{1}{M(E)} = \frac{1}{M_{\text{inelastic}}(E)} + \frac{1}{M_{\text{elastic}}(E)}. \quad (5)$$

The free parameters of the fitting are C_1 , M_0 , and C_2 in the $M(E)$ function and δ in the RTE model. The initial kinetic energy of o -Ps E_0 is assumed to be within the range of 0.8–3.0 eV [24,47]. All the measured data are simultaneously fitted, and chi-square for the previous experiments shown in Fig. 3(a) is also considered in the minimizing function.

The fitting curves are superimposed on the data in Fig. 2(b). All data are reasonably described by Eq. (5), which favors the quantum size effect model. The obtained parameters are $C_1 = 6.5_{-1.1}^{+0.6}$ (statistical) $_{-1.6}^{+2.7}$ (systematic) u eV, $M_0 = 0.6_{-0.6}^{+43}$ (statistical) $_{-0.6}^{+3}$ (systematic) u, $C_2 = 26 \pm 2$ (statistical) $_{-6}^{+8}$ (systematic) u eV, and $\delta = 0.1866 \pm 0.0007$ (statistical) $_{-0.0070}^{+0.0065}$ (systematic) nm, where u is the unified atomic mass unit. Here, the systematic uncertainties were estimated by considering the following factors: the assumption of E_0 and ε_{mn} , the measurement uncertainty of L , and the temperature distribution of the silica aerogel. The obtained δ is consistent with previous reports [37]. The fitted $M(E)$ function is superimposed in Fig. 3(a) with a 1σ uncertainty range (gray colored area) of $M(E)$ to which statistical and systematic uncertainties are combined. The function $M(E)$ is consistent with the previous experiments and the analysis with constant M for each T_{env} . Each component of the fitted Eq. (5) is shown in Fig. 3(b). The two steps of $M_{\text{inelastic}}$ at $E \approx 60$ meV and 140 meV are caused by the peaks of $k(\lambda)$ at $\lambda \approx 22$ μm and 9 μm , respectively, due to Si—O—Si resonance modes of vibration. The elastic contribution is dominant at T_{Ps} lower than room temperature, while the inelastic contribution becomes important at higher T_{Ps} . A global fitting only with the elastic contribution ends up with $\chi^2/\text{ndf} \approx 12$, which makes it necessary to include

the inelastic contribution. The simple model of the inelastic contribution used for the fitting is accurate enough in the range of the Ps kinetic energy of the present measurement and indispensable to reasonably explain the observed *o*-Ps thermalization process at cryogenic temperatures for the evaluation of the Ps cooling efficiency by thermalization.

The efficiency of Ps cooling by the thermalization process can now be evaluated with a good precision for T_{Ps} down to 100 K. It is revealed that the process is slower than the best-fit assumption in Ref. [19] due to the large M at low T_{Ps} . To evaluate the Ps cooling efficiency of a combination of the Ps thermalization and laser cooling, we simulated the time evolution of T_{Ps} based on Ref. [19] reflecting the results of this Letter. The simulation showed that the cooling efficiency was too low to realize Ps-BEC because it took twice as long time as the assumption in Ref. [19] to cool Ps down to ≈ 100 K, only below that temperature the laser cooling is effective. Halving L from 100 nm, which is used in Ref. [19], to 50 nm, which is still large enough to neglect the quantum confinement effect, can double the thermalization efficiency because the Ps energy loss rate is inversely proportional to L based on Eq. (2). Although a shorter L has a disadvantage of higher Ps pick-off annihilation rate which decreases the Ps density and BEC critical temperature, the Ps cooling simulation with $L = 50$ nm shows that the Ps cooling efficiency becomes high enough to realize Ps-BEC. Based on recent experiments of laser excitation of Ps confined in porous materials [44,48,49], laser cooling of Ps by $1S-2P$ transitions proposed in Ref. [19] might

have an obstacle because of the shortened lifetime of excited Ps inside the pores. Detailed understanding of interactions between excited Ps and porous materials is necessary for future laser cooling experiment of Ps confined in a silica cavity.

In summary, cooling of *o*-Ps down to 100 K in cryogenic silica aerogel has been performed and the time evolution of the *o*-Ps temperature has been measured by the pick-off technique. We have not only observed that the thermalization process becomes slower for Ps with less kinetic energy even in the silica cavities free from already suggested mechanisms for the lack of Ps thermalization at cryogenic temperatures but also identified the quantum size effect which can explain the measured slow thermalization with good agreement. This measurement has significantly decreased the uncertainty of the proposed cooling method, so we conclude that production of an *o*-Ps BEC is confirmed to be feasible by this method once laser cooling of Ps confined in silica cavity is realized.

The authors thank Dr. Koji Michishio and Dr. Ken Wada for useful discussions, especially about positronium physics. The authors are also grateful to Dr. Tomohiro Matsui and Dr. Kazushi Yawata for their help on the BET measurement. Sincere gratitude is expressed to Mr. Tomoyuki Murayoshi, Prof. Kosuke Yoshioka, and Prof. Makoto Kuwata-Gonokami for their excellent work on Ps laser cooling. This work was supported by JSPS KAKENHI Grants No. JP17H02820, No. JP17H06205, No. JP17J03691, No. JP19H01923, and the TIA Kakehashi Program No. TK17-046.

- [1] S. G. Karshenboim, Precision physics of simple atoms: QED tests, nuclear structure and fundamental constants, *Phys. Rep.* **422**, 1 (2005).
- [2] M. S. Fee, S. Chu, A. P. Mills, Jr., R. J. Chichester, D. M. Zuckerman, E. D. Shaw, and K. Danzmann, Measurement of the positronium $1^3S_1-2^3S_1$ interval by continuous-wave two-photon excitation, *Phys. Rev. A* **48**, 192 (1993).
- [3] A. Ishida, T. Namba, S. Asai, T. Kobayashi, H. Saito, M. Yoshida, K. Tanaka, and A. Yamamoto, New precision measurement of hyperfine splitting of positronium, *Phys. Lett. B* **734**, 338 (2014).
- [4] Y. Kataoka, S. Asai, and T. Kobayashi, First test of $O(\alpha^2)$ correction of the orthopositronium decay rate, *Phys. Lett. B* **671**, 219 (2009).
- [5] A. H. Al-Ramadhan and D. W. Gidley, New Precision Measurement of the Decay Rate of Singlet Positronium, *Phys. Rev. Lett.* **72**, 1632 (1994).
- [6] S. Asai, S. Orito, K. Yoshimura, and T. Haga, Search for Long-Lived Neutral Bosons in Orthopositronium Decay, *Phys. Rev. Lett.* **66**, 2440 (1991).
- [7] L. Gurung, T. J. Babij, S. D. Hogan, and D. B. Cassidy, Precision Microwave Spectroscopy of the Positronium $n = 2$ Fine Structure, *Phys. Rev. Lett.* **125**, 073002 (2020).
- [8] L. Gurung, T. J. Babij, J. Pérez-Ríos, S. D. Hogan, and D. B. Cassidy, Observation of asymmetric line shapes in precision microwave spectroscopy of the positronium $2^3S_1 \rightarrow 2^3P_J$ ($J = 1, 2$) fine-structure intervals, *Phys. Rev. A* **103**, 042805 (2021).
- [9] T. Yamazaki, T. Namba, S. Asai, and T. Kobayashi, Search for CP Violation in Positronium Decay, *Phys. Rev. Lett.* **104**, 083401 (2010).
- [10] A. P. Mills Jr. and M. Leventhal, Can we measure the gravitational free fall of cold Rydberg state positronium? *Nucl. Instrum. Methods Phys. Res. B* **192**, 102 (2002).
- [11] D. B. Cassidy and A. P. Mills, Jr., Physics with dense positronium, *Phys. Status Solidi C* **4**, 3419 (2007).
- [12] P. Crivelli, D. A. Cooke, and S. Friedreich, Experimental considerations for testing antimatter antigravity using positronium $1S-2S$ spectroscopy, *Int. J. Mod. Phys.: Conf. Series* **30**, 1460257 (2014).
- [13] S. Mariazzi, R. Caravita, M. Doser, G. Nebbia, and R. S. Brusa, Toward inertial sensing with a 2^3S positronium beam, *Eur. Phys. J. D* **74**, 79 (2020).
- [14] The ALPHA Collaboration and A. E. Charman, Description and first application of a new technique to measure the gravitational mass of antihydrogen, *Nat. Commun.* **4**, 1785 (2013).
- [15] P. Pérez, D. Banerjee, F. Biraben, D. Brook-Roberge, M. Charlton, P. Cladé, P. Comini, P. Crivelli, O. Dalkarov, P. Debu *et al.* (GBAR collaboration), The GBAR antimatter gravity experiment, *Hyperfine Interact.* **233**, 21 (2015).
- [16] M. Doser, C. Amsler, A. Belov, G. Bonomi, P. Bräunig, J. Bremer, R. Brusa, G. Burkhardt, L. Cabaret, C. Canali *et al.* (AEGIS Collaboration), Exploring the WEP with a pulsed cold beam of antihydrogen, *Class. Quantum Grav.* **29**, 184009 (2012).
- [17] C. Amsler, M. Antonello, A. Belov, G. Bonomi, R. S. Brusa, M. Caccia, A. Camper, R. Caravita, F. Castelli, P. Cheinet *et al.* (AEGIS Collaboration), Pulsed production of antihydrogen, *Commun. Phys.* **4**, 19 (2021).
- [18] P. M. Platzman and A. P. Mills, Jr., Possibilities for Bose condensation of positronium, *Phys. Rev. B* **49**, 454 (1994).

- [19] K. Shu, X. Fan, T. Yamazaki, T. Namba, S. Asai, K. Yoshioka, and M. Kuwata-Gonokami, Study on cooling of positronium for Bose-Einstein condensation, *J. Phys. B: At. Mol. Opt. Phys.* **49**, 104001 (2016).
- [20] A. Ishida, K. Shu, T. Murayoshi, X. Fan, T. Yamazaki, T. Namba, S. Asai, K. Yoshioka, and M. Kuwata-Gonokami, Monte Carlo simulation of positronium cooling for Bose-Einstein condensation, in *Poster Session at 14th International Workshop on Slow Positron Beam Techniques & Applications (SLOPOS14)* (The University of Tokyo, Tokyo, Japan, 2021), <https://doi.org/10.15083/0002000450>.
- [21] K. Shu, T. Murayoshi, X. Fan, A. Ishida, T. Yamazaki, T. Namba, S. Asai, K. Yoshioka, M. Kuwata-Gonokami, N. Oshima, B. E. O'Rourke, and R. Suzuki, Study on Bose-Einstein condensation of positronium, *J. Phys.: Conf. Ser.* **791**, 012007 (2017).
- [22] A. Ishida, K. Shu, T. Murayoshi, X. Fan, T. Namba, S. Asai, K. Yoshioka, M. Kuwata-Gonokami, N. Oshima, B. E. O'Rourke, and R. Suzuki, Study on positronium Bose-Einstein condensation, *JJAP Conf. Proc.* **7**, 011001 (2018).
- [23] A. P. Mills, Jr., Positronium Bose-Einstein condensation in liquid ^4He bubbles, *Phys. Rev. A* **100**, 063615 (2019).
- [24] Y. Nagashima, M. Kakimoto, T. Hyodo, K. Fujiwara, A. Ichimura, T. Chang, J. Deng, T. Akahane, T. Chiba, K. Suzuki, B. T. A. McKee, and A. T. Stewart, Thermalization of free positronium atoms by collisions with silica-powder grains, aerogel grains, and gas molecules, *Phys. Rev. A* **52**, 258 (1995).
- [25] T. Chang, M. Xu, and X. Zeng, Effect of the energy loss process on the annihilation of orthopositronium in silica aerogel, *Phys. Lett. A* **126**, 189 (1987).
- [26] Y. Nagashima, T. Hyodo, K. Fujiwara, and A. Ichimura, Momentum-transfer cross section for slow positronium-He scattering, *J. Phys. B: At. Mol. Opt. Phys.* **31**, 329 (1998).
- [27] K. Shibuya, Y. Kawamura, and H. Saito, Time-resolved determination of ortho-positronium kinetic energy utilizing p -wave scattering during positronium-xenon collisions, *Phys. Rev. A* **88**, 042517 (2013).
- [28] A. P. Mills, Jr., E. D. Shaw, R. J. Chichester, and D. M. Zuckerman, Positronium thermalization in SiO_2 powder, *Phys. Rev. B* **40**, 2045 (1989).
- [29] S. Mariuzzi, P. Bettotti, and R. S. Brusa, Positronium Cooling and Emission in Vacuum from Nanochannels at Cryogenic Temperature, *Phys. Rev. Lett.* **104**, 243401 (2010).
- [30] F. Guatieri, S. Mariuzzi, L. Penasa, G. Nebbia, C. Hugenschmidt, and R. S. Brusa, Time-of-flight apparatus for the measurement of slow positronium emitted by nanochannel converters at cryogenic temperatures, *Nucl. Instrum. Methods Phys. Res. B* **499**, 32 (2021).
- [31] S. Mariuzzi, A. Salemi, and R. S. Brusa, Positronium cooling into nanopores and nanochannels by phonon scattering, *Phys. Rev. B* **78**, 085428 (2008).
- [32] D. B. Cassidy, P. Crivelli, T. H. Hisakado, L. Liskay, V. E. Meline, P. Perez, H. W. K. Tom, and A. P. Mills, Jr., Positronium cooling in porous silica measured via Doppler spectroscopy, *Phys. Rev. A* **81**, 012715 (2010).
- [33] P. Crivelli, U. Gendotti, A. Rubbia, L. Liskay, P. Perez, and C. Corbel, Measurement of the orthopositronium confinement energy in mesoporous thin films, *Phys. Rev. A* **81**, 052703 (2010).
- [34] S. Asai, S. Orito, and N. Shinohara, New measurement of the orthopositronium decay rate, *Phys. Lett. B* **357**, 475 (1995).
- [35] A. Ishida, T. Namba, and S. Asai, Measurement of positronium thermalization in isobutane gas for precision measurement of ground-state hyperfine splitting, *J. Phys. B: At. Mol. Opt. Phys.* **49**, 064008 (2016).
- [36] K. Ito, H. Nakanishi, and Y. Ujihira, Extension of the equation for the annihilation lifetime of *ortho*-positronium at a cavity larger than 1 nm in radius, *J. Phys. Chem. B* **103**, 4555 (1999).
- [37] T. L. Dull, W. E. Frieze, D. W. Gidley, J. N. Sun, and A. F. Yee, Determination of pore size in mesoporous thin films from the annihilation lifetime of positronium, *J. Phys. Chem. B* **105**, 4657 (2001).
- [38] K. Wada and T. Hyodo, A simple shape-free model for pore-size estimation with positron annihilation lifetime spectroscopy, *J. Phys.: Conf. Ser.* **443**, 012003 (2013).
- [39] K. S. W. Sing, D. H. Everett, R. A. W. Haul, L. Moscou, R. A. Pierotti, J. Rouquerol, and T. Siemieniowska, Reporting physisorption data for gas/solid systems, in *Handbook of Heterogeneous Catalysis*, edited by G. Ertl, H. Knözinger, F. Schüth, and J. Weitkamp (Wiley-VCH Verlag GmbH & Co. KGaA, Weinheim, Germany, 2008), Chap. 3.3.1, pp. 1217–1230.
- [40] S. Agostinelli, J. Allison, K. Amako, J. Apostolakis, H. Araujo, P. Arce, M. Asai, D. Axen, S. Banerjee, G. Barrand *et al.* (GEANT4 Collaboration), GEANT4—a simulation toolkit, *Nucl. Instrum. Methods Phys. Res. A* **506**, 250 (2003).
- [41] J. Allison, K. Amako, J. Apostolakis, H. Araujo, P. Arce Dubois, M. Asai, G. Barrand, R. Capra, S. Chauvie, R. Chytracsek *et al.* (GEANT4 Collaboration), Geant4 developments and applications, *IEEE Trans. Nucl. Sci.* **53**, 270 (2006).
- [42] J. Allison, K. Amako, J. Apostolakis, P. Arce, M. Asai, T. Aso, E. Bagli, A. Bagulya, S. Banerjee, G. Barrand *et al.* (GEANT4 Collaboration), Recent developments in GEANT4, *Nucl. Instrum. Methods Phys. Res. A* **835**, 186 (2016).
- [43] P. G. Coleman, T. C. Griffith, and G. R. Heyland, The analysis of data obtained with time to amplitude converter and multi-channel analyser systems, *Appl. Phys.* **5**, 223 (1974).
- [44] B. S. Cooper, J.-P. Boilot, C. Corbel, F. Guillemot, L. Gurung, L. Liskay, and D. B. Cassidy, Annihilation of positronium atoms confined in mesoporous and macroporous SiO_2 films, *Phys. Rev. B* **97**, 205302 (2018).
- [45] P. Scheuerpflug, M. Hauck, and J. Fricke, Thermal properties of silica aerogels between 1.4 and 330 K, *J. Non-Cryst. Solids* **145**, 196 (1992).
- [46] R. Kitamura, L. Pilon, and M. Jonasz, Optical constants of silica glass from extreme ultraviolet to far infrared at near room temperature, *Appl. Opt.* **46**, 8118 (2007).
- [47] Y. Nagashima, Y. Morinaka, T. Kurihara, Y. Nagai, T. Hyodo, T. Shidara, and K. Nakahara, Origins of positronium emitted from SiO_2 , *Phys. Rev. B* **58**, 12676 (1998).
- [48] L. Gurung, B. S. Cooper, S. D. Hogan, and D. B. Cassidy, Resonant shifts of positronium energy levels in MgO powder, *Phys. Rev. A* **101**, 012701 (2020).
- [49] L. Gurung, T. J. Babij, and D. B. Cassidy, Fast decay of 2^3S_1 positronium atoms in an MgO lined cavity, *EPJ Tech. Instrum.* **8**, 3 (2021).